2023 IMEKO TC-4 International Conference on
Metrology for Archaeology and Cultural Heritage
Rome, Italy, October 19-21, 2023

The diagnostic study of the plaster casts of the Trajan's Column in the Museum of Roman Civilisation (Rome)

Federica Bubola[1], Chiara Coletti[1], Eleonora Balliana[2], Claudia Cecamore[3], Claudio Parisi Presicce[3], Claudio Mazzoli[1]

[1] *Department of Geosciences, University of Padua, Via Gradenigo 6, Padua, Italy, federica.bubola@phd.unipd.it, chiara.coletti@unipd.it, claudio.mazzoli@unipd.it*
[2] *Department of Environmental Sciences, Informatics and Statistics, Ca'Foscari University, Via Torino 155, Mestre, Italy, eleonora.balliana@unive.it*
[3] *Sovrintendenza Capitolina ai Beni Culturali, Piazza Lovatelli 35, Rome, Italy, claudia.cecamore@comune.roma.it, claudio.parisipresicce@comune.roma.it*

Abstract
In recent years, the control of the microclimate in museums has been increasingly recognised as important. This research focuses on state of conservation assessment of 34 plaster casts of Trajan's Column at the Museum of Roman Civilisation and on the microclimate monitoring of the Room LI, where they are conserved. The results continue to demonstrate that the main causes of decay derive from unsuitable climate conditions, which lead to cracks and detachments.

I. INTRODUCTION

The control of the microclimate in museum environments or historical buildings is a fundamental aspect in the protection of artefacts and the planning of an appropriate conservation strategy. Deterioration processes, defined as a result of progressive and cumulative material decay, depends on environmental variables and their changes. In particular, inappropriate temperature and relative humidity levels speed up chemical and physical deterioration and may cause irreversible decay to cultural artefacts.

Variations in hygrothermic conditions can generate physical and structural changes on the surface, influence and catalyse chemical reactions, i.e. hydrolysis and oxidation-reduction [1], and cause biodeterioration. Gypsum-based plaster artefacts may undergo issues such as deformations, loss of adhesion and in general structural and mechanical changes, solubilisation, migration and salt crystallisation.

The plaster casts of the Trajan's Column, made by Napoleon III between 1861 and 1862, are the object of this study.

In view of the imminent reopening of the Museum of Roman Civilisation (MCR) and the restoration of its plaster casts, the assessment of the current microclimate quality is crucial for long-term preservation of them.

II. MATERIALS AND METHODS

A. Experimental strategy

The complete set of plaster casts reproducing the Trajan's Column, has been housed in Room LI at the Museum of Roman Civilisation since around the mid-1900s. Unfortunately, limited information is available regarding their previous state of conservation. The current study of the microclimate enables a comparison between the current state of preservation and the condition of the plaster casts in 2012, year in which the Museum conducted a conservation survey campaign.

In this first research phase of the microclimate monitoring campaign in the Museum, a sensor was placed for a period of approximately seven months. Climate data was collected from November 23, 2022, to June 8, 2023, for a total of 4407 readings.

In this study 34 plaster casts were analysed (the complete set reproducing the Trajan's Column counts 125 plasters). A photographic campaign was carried out to identify and highlight the details and main visible causes of degradation. The images acquired were used to support the decay mapping carried out for each cast. The on-site macroscopic investigation was supported by the use of the Dino-Lite contact optical microscope, both in natural and ultraviolet light. In addition, InfraRed Thermography was applied to investigate detachments and cracks.

Two micro-samples, in the form of small spalling (samples A and B) were collected from the MCR_3045 plaster cast. The samples were analysed using different analytical methodologies: X-Ray Powder Diffraction (XRPD) was used in order to identify the mineral phases; Field Emission Scanning Electron Microscopy (FESEM) to investigate the mineralogy and morphology of the samples; Attenuated Total Reflection Infrared Spectroscopy (ATR-FTIR) performed qualitative analyses for the identification of organic and inorganic compounds;

and μ-Raman spectroscopy was applied to identify the composing materials.

B. Microclimatic monitoring

The microclimatic monitoring was carried out using an OM-EL-USB-2LCD by OMEGA® data logger. Monitoring was performed recording climate data with a frequency of 30 minutes.

C. Analytical Techniques

The photographs were taken with a Canon camera under lighting conditions using 230V 750W halogen lamps. White balance was carried out in situ directly from the camera.

Thermal diffusion was studied using an InfraRed-Thermocamera (FLIR). InfraRed-images were captured in time lapse mode every 30s (41 frame total) after heating the plaster casts with halogen lamps for 20 min at a distance of 1m. The IR-images and the profiles of thermal diffusion were extrapolated using FLIR ResearchIR 4 Max + HSDR software® Images were saved in false colour with palette GF White Hot function, in the thermal range of 11-35°C using the FLIR system DDE (Digital Detail Enhancement) algorithm.

Diffraction data were acquired on a PANalytical X'Pert PRO diffractometer operating in Bragg-Brentano reflection geometry with CoKα radiation, 40kV voltage and 40mA filament current, equipped with an X'Celerator detector. Qualitative analysis of diffraction data was carried out with X'Pert HighScore Plus® software (PANalytical) and the PDF-2 database.

Raman measurements were made using a Thermo Scientific DXR Raman Microscope using a 532nm laser excitation source. Analyses were performed using a 50x long working distance objective with ~2.5cm^{-1} spectral resolution, ~1μm pinhole operating at 3mW of power. To minimize noise, each spectrum was acquired 30 times with an exposure time of 1s. Spectra were recorded in the frequency range from 100 to 3500cm^{-1}. Spectral fitting was carried out using the Thermo Scientific OMNIC Spectra Software (Version 9) and then processed with OriginPRO 2018b.

For the Attenuated Total Reflection Infrared Spectroscopy, a Bruker ALPHA II by Bruker Optics® Fourier transform IR Spectrometer was used. ATR-FTIR analyses were recorded in the spectral range from 4000 to 400cm^{-1}, using a synthetic diamond crystal for sample compression. The background was measured with 48 scans before each acquisition, while the samples were analysed with 48 scans, with a resolution of 4cm^{-1}. The spectra obtained were processed with the Thermo Scientific OMNIC Spectra Software (Version 9), and then further processed with OriginPRO 2018b.

Sample mineralogy and morphology were investigated with a FESEM Tescan Solaris. Microchemical analysis was performed on mineral phases as observed under the FESEM, using an Oxford Instrument Ultim Max 65 Silicon drift detector EDS and operating at 15KeV with a current of 3nA and a working distance of 5mm. Backscattered electron (BSE) images were acquired working at lower tension and current (5KeV, 300 pA and at a working distance of 4mm) to improve image resolution.

III. RESULTS AND DISCUSSION

A. Experimental strategy

The temperature graph in Fig.1A shows a curve devoid of fluctuations and significant peaks with an average value of 14.06°C. The minimum value reached on 10 February 2023 is 8°C, while the maximum value of 26°C was reached on 7 June 2023.

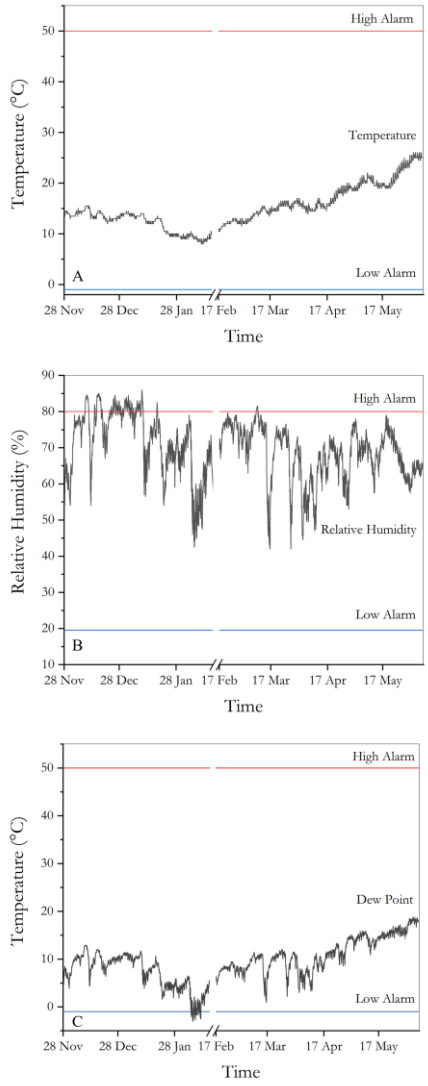

Figure 1. Temperature (A), Relative Humidity (B) and Dew Point (C) data obtained from the microclimatic monitoring of Room LI, over a period of seven moths.

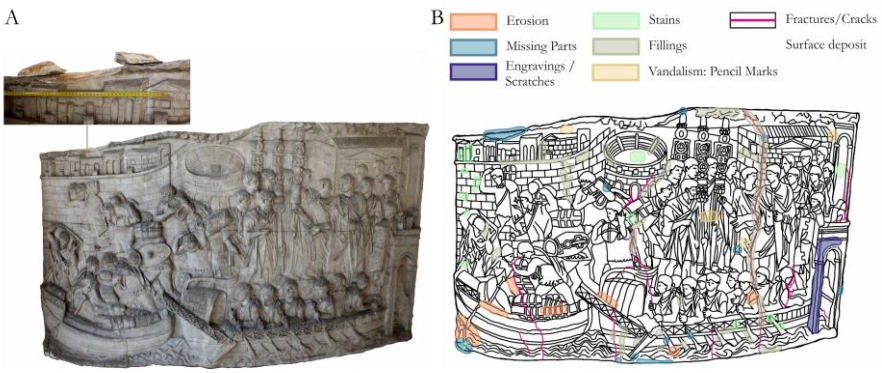

Figure 2. Plaster cast MCR_3045, with a detail of missing part from which sample A was taken (A). Degradation map of the MCR_3045 plaster cast and the legend showing the degradation patterns (B).

The relative humidity data (Fig.1B) shows a non-linear trend, with the presence of numerous peaks and fluctuations. Daily fluctuations in relative humidity are influenced by the day-night cycle, with a strong relationship between relative humidity and temperature: low temperatures correspond to an increase in relative humidity, particularly in the early morning hours. The sensor was set in a range between 19.5% and 80.0%. The RH levels exceeded the maximum set level of 80% numerous times. The minimum value of RH% was recorded on the evening of 28 March 2023 and is 42%, while the maximum value is 86%, recorded on 9 January 2023.

The acquired dew point data (Fig.1C) show that the minimum value was reached on 6 February 2023 at 11 p.m., and was -3°C, while the maximum value was reached on 23 November 2022 at 1 p.m., and was 18.8°C.

B. Plaster casts characterisation

In the 2012 campaign to survey their conservation state, the 125 gypsum-based plaster casts have been divided into three classes, depending on the typology and the severity of the degradation patterns (mediocre, discreet and poor). From each of these classes, ten casts were selected to be studied. Moreover, four other plaster casts which did not fit into one of the classes were selected. The analysed plaster casts were chosen on the basis of the institution's requirements, their state of preservation and their location within the gallery.

The casts consist of sections, held together by a wooden and metal structure placed on the back. This complex structure of heterogeneous materials can react with the surrounding environment under very humid conservative conditions, and in the presence of liquid water can cause specific decay patterns. In fact, the presence of rust stains was observed both on the back and on the surface of the casts. In general, the surface of the casts is covered by coherent deposits, particularly in the most exposed areas, due to the porosity and hygroscopicity of gypsum, which are mainly responsible for the tendency of this material to retain dust. In addition, diffuse yellow and pink tonal variations are present, probably due to historical patinas. Pencil marks are present in some areas, while surface scratches cover most of the surface of the casts. All the plaster casts, especially those belonging to the discreet and poor classes show presence of micro-cracks and deep fractures, some of which extended over almost the entire height. In addition to the rust stains, a large amount of dark-coloured and red/brown stains of different size, and residues of mortar are visible, probably related to the modelling of the casts (Fig.2). Several casts also display areas subjected to erosion, pulverisation and lifting.

The thermograms emphasise detachments and cracks [2]. In Fig.3B, the area underneath, having absorbed less heat, shows a dark colour, while the more exposed surface area is highlighted by a strong yellow colour, since it has absorbed more heat, as it is closer to the source.

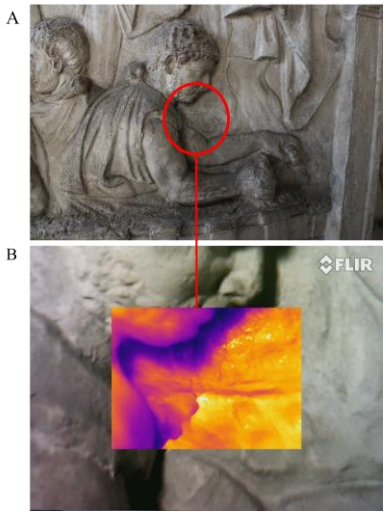

Figure 3. Detail of a fracture in the MCR_3045 plaster cast (A). Thermogram acquisition highlighting the deep fracture with the uplift of the material (B).

The mineralogical characterisation by XRPD analysis (Fig.4A) on the collected samples (Fig.5A) showed that the main constituent material is gypsum ($CaSO_4 \cdot 2H_2O$) indicated by the presence of the characteristic diffraction peaks (*Gp)*, marked with approved mineral symbols [3,4]. The diffractogram of sample A shows the presence of gypsum and calcite ($CaCO_3$). The analysis also showed traces of quartz and kaolinite ($Al_2Si_2O_5(OH)_4$). The diffractogram of sample B, shows only the presence of gypsum and quartz (SiO_2).

FESEM analyses confirmed what was drawn by mineralogical characterisation. The matrix of the sample is characterised by a heightened porosity in the bulk, while a more compact gypsum morphology characterises the surface layer. Analyses confirmed quartz and kaolinite inclusions characterised by the presence of Al, Si and K. The presence of these elements revealed also a surface finishing layer highlighted in green in the map (Fig.4B), mainly composed of kaolinite.

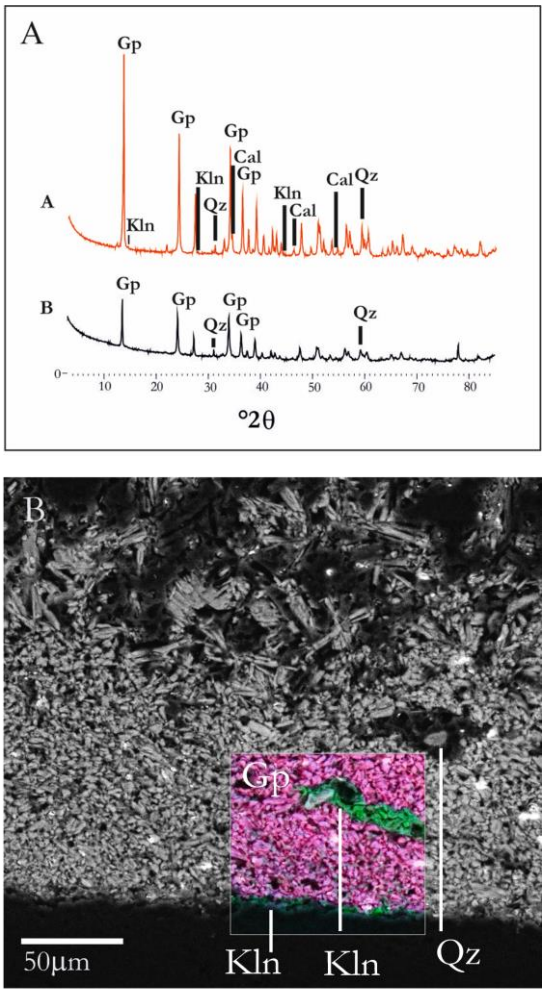

Figure 4. XRPD patterns of sample A and B (A); FESEM image of sample B. The map highlights less porous gypsum-based matrix with inclusions of quartz and kaolinite, and a finishing rich in kaolinite (B).

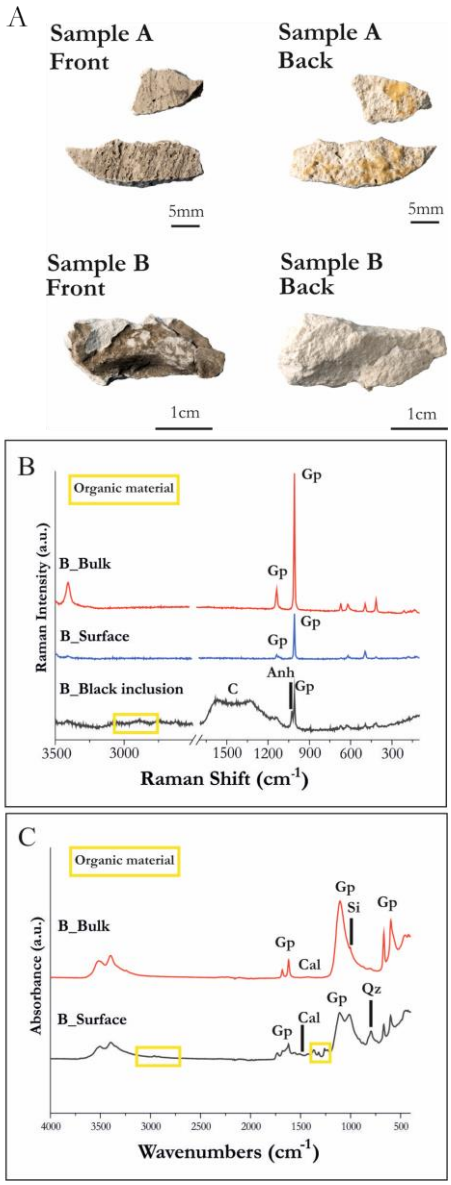

Figure 5. Micro-samples (samples A and B, front and back) collected from the plaster cast MCR_3045 (A). Raman spectra of sample B (B); ATR-FTIR spectra of sample B (C).

The three µRaman spectra show the characteristic bands of gypsum at 1140, 1008, 673, 492 and 414 cm^{-1}, corresponding to the stretch vibrational mode of SO_4 (Fig.5B) [5,6]. The two Raman bands observed around 3405 and 3490 cm^{-1} correspond to the O-H stretching vibration of water molecules in gypsum. The spectra show traces of anhydrite, with the characteristic bands of the sulphate ions at 1170, 1026 and 630 cm^{-1}. The presence of anhydrite can be ascribed to the raw material used in the moulding of the casts [6].

ATR-FTIR spectra of sample B, determined the presence of gypsum ($CaSO_4 \cdot 2H_2O$) by the peaks at 1680, 1620 cm^{-1} (bending OH), and at 1110, 670 and 620 cm^{-1} (Fig.5C). These peaks correspond to the

stretching vibration of SO_4^{2-}, while the stretching vibrations of the water molecules of the gypsum occur at ~3500 and ~3400 cm^{-1} [7].

The peak at 3340 cm^{-1} in the spectrum of the surface corresponds instead at the stretching OH of non-bonding water molecules. The carbonate functional group relates to the presence of calcite can be detected in both the spectra due to the presence of the characteristic peaks at ~1420-1430 and 873 cm^{-1} [8]. The broad low intensity in the range 800-770 cm^{-1} could be ascribed to the presence of quartz, present in the raw material or added during the moulding process [9]. The bands at 2964, 2920, 2850 cm^{-1} can be related to the stretching CH of an organic substance, as well as the peaks at 1736 cm^{-1} (stretching C=O), 1562 and 1511 cm^{-1} (stretching C-C), and the bands at ~1370 and 1230 cm^{-1} (bending CH) [10]. This organic material can be attributed to some compound used in previous intervention or as a finishing.

IV. CONCLUSION

The microclimate data recorded in the period between November 2023 and June 2023 show an average temperature of 15.06°C, with relative humidity levels occasionally exceeding 80%. When compared to the 2012 reports, it becomes evident that environmental conditions, especially fluctuations in relative humidity, have had a significant impact on the state of preservation of the gypsum-based plaster casts. This impact is evident in the development of various forms of degradation, including new fractures, erosion, and material pulverisation. Additionally, the surfaces exhibit scratches, deposits, and stains.

These results will support the restoration efforts for the plasters casts, ensuring their optimal preservation once the Museum reopens.

Some ongoing analyses include on-site Hyperspectral Imaging to map and confirm forms of degradation such as the presence of biological attacks; colorimetric measurements to understand tonal variations on the surfaces of the plaster casts; and Thermogravimetry-Differential Scanning Calorimetry and Pyrolysis Gas-Chromatography to identify organic materials.

Furthermore, a result of a structural analysis of Room LI will be conducted using IR Thermography. Based on the results of this analysis, a comprehensive microclimatic monitoring campaign will be initiated, employing higher-performance sensors, strategically positioned at critical points within the gallery.

REFERENCES

[1] A. Spagnulo, C. Vetromile, A. Masiello, M.F. Alberghina, S. Schiavone, C. Lubritto, “Climate and Cultural Heritage: The Case Study of “Real Sito of Carditello”, Heritage, vol.2, No.3, July 2019, pp. 2053-2066.

[2] F. Mercuri, U. Zammit, N. Orazi, S. Paoloni, M. Marinelli, F. Scudieri, “Active infrared thermography applied to the investigation of art and historic artefacts”, J. Therm. Anal. Calorim., May 2011, vol.104, No.2, pp. 475-485.

[3] J. C. A. Boeyens, V. V. H. Ichharam, “Redetermination of the crystal structure of calcium sulphate dihydrate, $CaSO_4 \cdot 2H_2O$”, Z. Kristallogr., vol.217, January 2002, pp. 9-10.

[4] L. N Warr, “IMA-CNMNC approved mineral symbols”, Mineral Mag., vol.85, No.3, June 2021, pp. 291-320.

[5] V. Antunes, A. Candeias, M. J. Oliveira, S. Longelin, V. Serrão, A. I. Seruya, J. Coroado, L. Dias, J. Mirão, M. L. Carvalho, “Characterization of gypsum and anhydrite ground layers in 15th and 16th centuries Portuguese paintings by Raman Spectroscopy and other techniques”, J. Raman Spectrosc., vol.45, No.11-12, November 2014, pp. 1026-1033.

[6] N. Prieto-Taboada, O. Gómez-Laserna, I. Martínez-Arkarazo, M. A. Olazabal, J. M. Madariaga, “Raman Spectra of the Different Phases in the $CaSO_4$-H_2O System”, Anal. Chem., vol.86, No.20, October 2014, pp. 10131-10137.

[7] D. Gramtorp, K. Botfeldt, J. Glastrup, K. P. Simonsen, “Investigation of Anne Marie Carl-Nielsen’s waz models, Stud. Conserv., vol.60, No.2, March 2015, pp. 97-106.

[8] F. A. Andersen, L. Brečevic, “Infrared Spectra of Amorphous and Crystalline Calcium Carbonate”, Acta Chem. Scand., vol.45, 1991, pp. 1018-1024.

[9] I. Fikri, M. El Amraoui, M. Haddad, A. S. Ettahiri, C. Falguères, L. Bellot-Gurlet, T. Lamhasni, S. A. Lyazidi, L. Bejjit, “Raman and ATR-FTIR analyses of medieval wall paintings from al-Qarawiyyin in Fez (Morocco)”, SAA, June 2022.

[10] F. Pozzi, E. Basso, S. Alderson, J. Levinson, M. Neimar, S. Alcalá, “Aiding the cleaning of four 19th-century Tsimshian house posts: investigation of museum-applied surface coatings and original polychromy”, Herit. Sci., vol.9, No.42, December 2021.